

Boise State University

ScholarWorks

Civil Engineering Faculty Publications and
Presentations

Department of Civil Engineering

3-16-2022

Benthic Biolayer Structure Controls Whole-Stream Reactive Transport

Kevin R. Roche

Boise State University

Marco Dentz

Spanish National Research Council (IDAEA-CSIC)

Geophysical Research Letters®

RESEARCH LETTER

10.1029/2021GL096803

Key Points:

- Storage in non-reactive sublayer causes long contaminant survival times
- Reach-scale reaction kinetics cannot be captured by constant rate model
- Upscaled model quantifies all aspects of reaction and mass transfer

Supporting Information:

Supporting Information may be found in the online version of this article.

Correspondence to:

K. R. Roche,
kevinroche@boisestate.edu

Citation:

Roche, K. R., & Dentz, M. (2022). Benthic biolayer structure controls whole-stream reactive transport. *Geophysical Research Letters*, 49, e2021GL096803. <https://doi.org/10.1029/2021GL096803>

Received 27 OCT 2021

Accepted 23 FEB 2022

Benthic Biolayer Structure Controls Whole-Stream Reactive Transport

Kevin R. Roche^{1,2}  and Marco Dentz¹ 

¹Spanish National Research Council (IDAEA-CSIC), Barcelona, Spain, ²Department of Civil Engineering, Boise State University, Boise, ID, USA

Abstract Hyporheic zone reaction rates are highest just below the sediment-water interface, in a shallow region called the benthic biolayer. Vertical variability of hyporheic reaction rates leads to unexpected reaction kinetics for stream-borne solutes, compared to classical model predictions. We show that deeper, low-reactivity locations within the hyporheic zone retain solutes for extended periods, which delays reactions and causes solutes to persist at higher concentrations in the stream reach than would be predicted by classical approaches. These behaviors are captured by an upscaled model that reveals the fundamental physical and chemical processes in the hyporheic zone. We show how time scales of transport and reaction within the biolayer control solute retention and transformation at the stream scale, and we demonstrate that accurate assessment of stream-scale reactivity requires methods that integrate over all travel times.

Plain Language Summary Dissolved materials such as carbon, nutrients, and contaminants react as they move through the river network. Some locations in the river are far more reactive than others, and it is challenging to predict how this spatial variability of reaction rates controls the reactivity of the entire stream. One hotspot of high reactivity is the benthic biolayer, a thin region below the sediment-water interface with an abundance of microbial activity, and below which reactivity decreases to very low values. We use a mathematical model to quantify the benthic biolayer's contribution to whole river material transformation, based on the biolayer's thickness and reactivity. We show that thin or less reactive biolayers allow dissolved mass to become sequestered for long periods deep in the streambed, leading to low but persistent concentrations long after the mass is introduced to the river. These theoretical advances improve our understanding of how measurable features of the river—namely, the depth-dependent reaction rates within the streambed—are directly related to biogeochemical transformations and contaminant retention timescales in rivers.

1. Introduction

A defining feature of rivers is the transition in physical and chemical characteristics across the sediment-water interface (SWI). Downstream velocities, mixing rates, and available light decrease rapidly at the SWI to viscous flows and light limited conditions (Jones & Mulholland, 1999). This transition zone, called the benthic biolayer, contributes disproportionately to the biologically mediated transformation of solutes and fine particulate matter in the river corridor, including heterotrophic carbon respiration, nutrient cycling, and trace contaminant degradation (Battin et al., 2008; Kunkel & Radke, 2008; Marzadri et al., 2017). Fluvial ecosystems are highly sensitive to physical perturbations and elevated contaminant concentrations in the biolayer, since this region supplies refugia and energy (as microbial biomass) for freshwater vertebrates (Jones & Mulholland, 1999; Moran et al., 2017). Structural features of the biolayer, such as depth and reactivity, are therefore important predictors of whole-river reactivity and ecosystem health.

Dissolved oxygen depletes as aerated surface water propagates deeper into the hyporheic zone (HZ), leading to conditions that sustain microbial communities with higher tolerance for anoxia and slower metabolism. The stratification of chemical conditions and microbial biomass below the SWI creates sharp gradients in reaction rates, as well as regions of low reactivity below the biolayer (Harvey et al., 2013; Knapp et al., 2017; Kunkel & Radke, 2008). It is challenging to determine the vertical profile of reaction rates not only because steep concentration gradients are difficult to measure in pore waters, but also because various transport processes are simultaneously active (e.g., advective pumping, molecular and turbulent diffusion, mechanical dispersion). These processes are often grouped using scaling laws to estimate vertical solute fluxes across the SWI. Scaling predictions are related to subsurface concentrations by assuming that solutes diffuse vertically (Grant et al., 2012), which allows

the reaction profile to be inferred from a diffusion-reaction or similar 1-D transport model (Harvey et al., 2013; Knapp et al., 2017; Schaper et al., 2019).

Recent modeling efforts strongly suggest that spatial variability of reaction rates in the biolayer controls the fate of reactive solutes at the stream scale. Numerical simulations show that whole-stream transformation is 5–25× greater when HZ reaction rates are highest near the SWI, compared to a stream with the same vertically averaged reactivity uniformly distributed in the HZ (Li et al., 2017). These differences arise because solutes entering the HZ most commonly propagate through shallow, high reactivity flowpaths before returning to the water column. Process-based models must therefore account for the correlation between residence time in the stream and residence time in reactive regions of the river bed. Travel time based approaches for advection-dominated hyporheic flows account for the variability of reaction rates along flow paths by assuming that fluid parcels move unmixed through the HZ (Azizian et al., 2015; Reeder et al., 2018). However, we currently lack an upscaling framework that accounts for the joint impact of spatially varying reaction rates and diffusive mass transfer in the HZ. This knowledge gap limits our understanding of how measurable features of the HZ contribute to river corridor biogeochemistry, as well as how long streamborne contaminants are retained in low-reactivity regions below the biolayer that can act as a secondary source.

This work is motivated by the questions of how the size and reactivity of the benthic biolayer influence reach-scale mass fate, and how these properties manifest in upscaled observations of reactive transport. We isolate the effects of depth-dependent HZ reaction rates on upscaled predictions of solute fate in a stream. Solute transport in the HZ is considered to be dominated by vertical diffusion, which aligns our analysis with existing scaling laws that predict hyporheic exchange fluxes from measurable parameters. We present streambed- and reach-scale simulations designed to mimic a pulse tracer injection, which is a common method for assessing the processes controlling reactive transport in rivers and whose results are extendable to other boundary conditions that more closely represent plateau injection experiments or time-variable contaminant loading from non-point sources. We compare numerical results to predictions from a classical mobile-immobile model with uniform reactions in the subsurface, as well as predictions from a novel mobile-immobile model that explicitly represents the vertically varying reaction profile in the HZ.

2. Methods

2.1. Transport Scenario

The model domain comprises the water column and HZ (Figure 1). The SWI is located at $z = 0$, the water column extends from $z = 0$ to $z = d$, and the HZ extends from $z = -h$ to $z = 0$. The stream velocity is $v(z) = v_s + v_0\kappa^{-1} \ln(z/z_0)$ for $z > z_0$ and zero for $z < z_0$ (Fischer et al., 1979). The length z_0 is the width of a roughness layer at the SWI and represents the effect of the porous streambed on the stream velocity, $\kappa \approx 0.41$ is the von Karman coefficient, v_0 the shear velocity, and v_s the slip velocity at the SWI. We set $v(z) = 0$ in the HZ, which assumes that streamwise velocity in the HZ is negligible compared to the stream. Vertical mixing is quantified by the dispersion coefficient $D(z)$, which is set equal to $D(z) = \kappa v_0 z (1 - z/d)$ for $z > z_0$ in the water column (Fischer et al., 1979) and equal to the constant effective diffusivity D_h in the HZ. We disregard streamwise dispersion and diffusion because advection in the water column dominates streamwise transport.

Solutes undergo first-order reactions in the HZ, which is a reasonable assumption when reactions are independent of the concentration of co-reactants, abundance of catalysts such as enzymes, or thermodynamic constraints (Dodds et al., 2002; Garayburu-Caruso et al., 2020). Water column reactions can be easily incorporated into the analytical and numerical models presented here (e.g., Roche et al., 2019); however, we set $k(z > 0) = 0$ to elucidate the biolayer's influence on stream-scale reactivity. The depth-dependent reaction rate $k(z)$ can be an arbitrary function of streambed elevation, but typically decreases sharply with depth due to the presence of the benthic biolayer. We follow Li et al. (2017) and consider a biolayer structure consistent with field observations (Inwood et al., 2007; Knapp et al., 2017; Schaper et al., 2019). The reaction rate is set to $k(z) = k_b$ within a layer of thickness b just below the SWI. It is set to $k(z) = 0$ in the non-reactive sublayer of thickness $\ell = h - b$. Other profiles that decay on a characteristic length scale b are expected to show qualitatively similar behavior. The characteristic time scales in the HZ are given by the reaction time $\tau_r = k_b^{-1}$, as well as the diffusion times $\tau_h = h^2/D_h$ across the HZ, $\tau_b = b^2/D_h$ across the biolayer, and $\tau_\ell = \ell^2/D_h$ across the non-reactive sublayer. The Damköhler number $Da = \tau_b k_b$ compares diffusion and reaction times in the biolayer. We consider the order of time scales $\tau_r \leq \tau_b < \tau_\ell$,

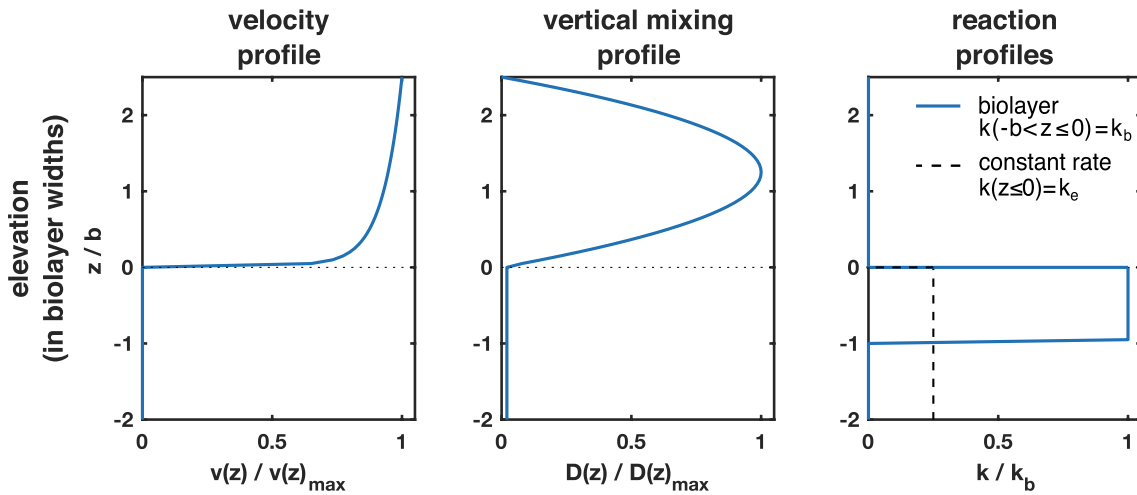


Figure 1. (Left to right) Spatial velocity, vertical mixing, and reaction profiles across the surface-subsurface continuum. The sediment-water interface is located at $z = 0$. Figures are truncated at $z/b = -2$ since all values are constant below this elevation.

such that $Da \geq 1$. This implies that reactions can occur before solute is transmitted to the sublayer. In contrast, if $\tau_r > \tau_b$ (i.e., $Da < 1$), very little solute will react before reaching the sublayer. Reactive and conservative solutes behave similarly in this case. The evolution of solute concentration $C(x, z, t)$ in the combined stream-HZ system is expressed by the advection-dispersion equation

$$\theta(z) \frac{\partial C}{\partial t} + v(z) \frac{\partial C}{\partial x} - \frac{\partial}{\partial z} \left[\theta(z) D(z) \frac{\partial C}{\partial z} \right] = -\theta(z) k(z) C, \quad (1)$$

where porosity $\theta(z)$ equals 1 in the water column and θ_h in the HZ. The horizontal boundaries $z = -h$ and $z = d$ are impermeable. Consistent with the experimental design of field tracer studies, we assume the HZ is initially free of reactive mass, and solute is introduced as a line injection in the water column. We perform direct numerical simulations to solve Equation 1 using a reactive time-domain random walk approach (TDRW), based on the implementation of Russian et al. (2016) for conservative solutes. The TDRW method is computationally efficient for media with spatially heterogeneous advection, diffusion and reaction properties. Details on the implementation, discretization, and parameterization of the TDRW simulations are given in Section SI-VI in the Supporting Information S1.

2.2. Mobile-Immobile Biolayer (MIM-B) Model

We use a mobile-immobile approach to upscale the reactive transport problem (Haggerty et al., 2002). Equation 1 is decomposed into an advection-dispersion equation for transport in the stream, a diffusion-reaction equation for the biolayer, and an equation for vertical diffusion in the sublayer. These equations are coupled through concentration and flux continuity at their respective interfaces. By vertical averaging we obtain a temporally non-local equation for average stream concentration ($\bar{C}_s(x, t) = \frac{1}{d} \int_0^d C(x, z, t) dz$):

$$\begin{aligned} \frac{\partial \bar{C}_s}{\partial t} + \frac{\theta_h}{d} \frac{\partial}{\partial t} \int_0^t dt' \varphi_h(t-t') \bar{C}_s(x, t') \\ + \bar{v} \frac{\partial \bar{C}_s}{\partial x} - D^* \frac{\partial^2 \bar{C}_s}{\partial x^2} = -\frac{\theta_h k_b}{d} \int_0^t dt' \varphi_h(t-t') \bar{C}_s(x, t'). \end{aligned} \quad (2)$$

The mean stream velocity \bar{v} and the shear dispersion coefficient $D^* = 5.93 v_0 d$ are determined directly through spatial averaging of the velocity and vertical mixing profiles in the water column (Fischer et al., 1979). The non-local term (second term on left side) denotes the time derivative of the concentration in the HZ and quantifies solute trapping, release, and degradation in the hyporheic zone. The right-hand-side term demonstrates that the upscaled reaction kinetics are temporally non-local, but nonetheless linear. The non-locality stems from the fact that solute first diffuses into the biolayer before it reacts. Thus, mass degraded at a given time t is proportional to the stream concentrations $\bar{C}_s(x, t')$ at earlier times t' . The memory kernel $\varphi_h(t)$ describes the evolution of mass

in the HZ in response to an instantaneous solute pulse at the SWI. It is decomposed into $\varphi_h(t) = \varphi_b(t) + \varphi_0(t)$, where $\varphi_b(t)$ and $\varphi_0(t)$ encode the diffusive and reactive mass transfer mechanisms across the biolayer and the non-reactive sublayer, respectively. Explicit Laplace space expressions for $\varphi_b(t)$ and $\varphi_0(t)$ are given in Section SI-IIC in the Supporting Information S1. We present solutions to Equation 2 for initial condition $\bar{C}_s(x, 0) = 0$ and the boundary condition, $\bar{C}_s(0, t) = \delta(t)$, to analyze solute breakthrough curves in the upscaled model. The linearity of the model allows it to accommodate alternative boundary conditions, such as those representing a time-varying or constant loading of contaminant.

2.3. Surrogate Models

To illustrate the benthic biolayer's impact on whole stream reactive transport, we contrast the MIM-B with two surrogate models, termed *S1* and *S2*. Model *S1* assumes the hyporheic zone is uniformly reactive over all depths. Model *S2* assumes that water column and HZ are in equilibrium.

2.3.1. Fully Reactive Hyporheic Zone (S1)

In agreement with classical assumptions (e.g., Haggerty et al., 2009; Runkel, 2007), *S1* assumes that the HZ is fully reactive and characterized by an equivalent reaction rate k_e . The evolution equation for \bar{C}_s is obtained from Equation 2 by substituting k_b with k_e and setting $\varphi_h(t) = \varphi_b(t) \equiv \varphi_e(t)$. The latter can be written in terms of the memory kernel $\phi(t)$ for a non-reactive solute as $\varphi_e(t) = \phi(t) \exp(-k_e t)$ (Dentz et al., 2011). We define k_e such that the total reacted mass in the HZ, in response to an instantaneous solute pulse at the SWI, is equal to the total reacted mass in the MIM-B. Using this definition, we derive the following transcendental equation for k_e (see SI-IV in the Supporting Information S1)

$$\sqrt{\frac{k_e}{k_b}} \tanh\left(\sqrt{k_e \tau_h}\right) = \tanh\left(\sqrt{Da}\right). \quad (3)$$

The solution of Equation 3 can be approximated by $k_e = k_b \tanh\left(\sqrt{Da}\right)^2$ for $k_e \tau_h > 10$. This implies that the equivalent streambed reactivity increases monotonically with Da and asymptotes toward k_b as $Da \rightarrow \infty$.

2.3.2. Equilibrium Model for the Water Column (S2)

Model *S2* assumes that the water column and the HZ are in equilibrium. The evolution equation for \bar{C}_s in this limit is obtained from Equation 2 by localization of the memory kernels on the left and right sides. This gives (Section SI-V in the Supporting Information S1)

$$R_a \frac{\partial \bar{C}_s}{\partial t} + \bar{v} \frac{\partial \bar{C}_s}{\partial x} - D^* \frac{\partial^2 \bar{C}_s}{\partial x^2} = -k_a \bar{C}_s(x, t'), \quad (4)$$

where the apparent retardation coefficient R_a and the apparent reaction rate k_a are defined by

$$R_a = 1 + \frac{\theta_h}{d} \int_0^\infty dt' \varphi_h(t'), \quad k_a = \frac{\theta_h k_b}{d} \int_0^\infty dt' \varphi_b(t'). \quad (5)$$

2.4. Reach-Scale Reactivity

The two surrogate models *S1* and *S2* have the same downstream mass recovery as the MIM-B model. The fraction of mass recovered M_R at a downstream location is obtained by integration of the solute breakthrough curves over all times. Thus, we obtain from *S2*:

$$M_R(x) = \exp \left[-\frac{x\bar{v}}{2D^*} \left(\sqrt{1 + \frac{4k_a D^*}{\bar{v}^2}} - 1 \right) \right]. \quad (6)$$

This predicted exponential decrease is commonly observed in field experiments. The reach scale reactivity K_r [L^{-1}] has been defined in the literature as the slope of the logarithm of $M_R(x)$, that is, $K_r \equiv -x^{-1} \ln M_R(x)$ (Tank et al., 2008). Reach scale reactivity K_r reads in terms of the apparent reaction rate k_a as

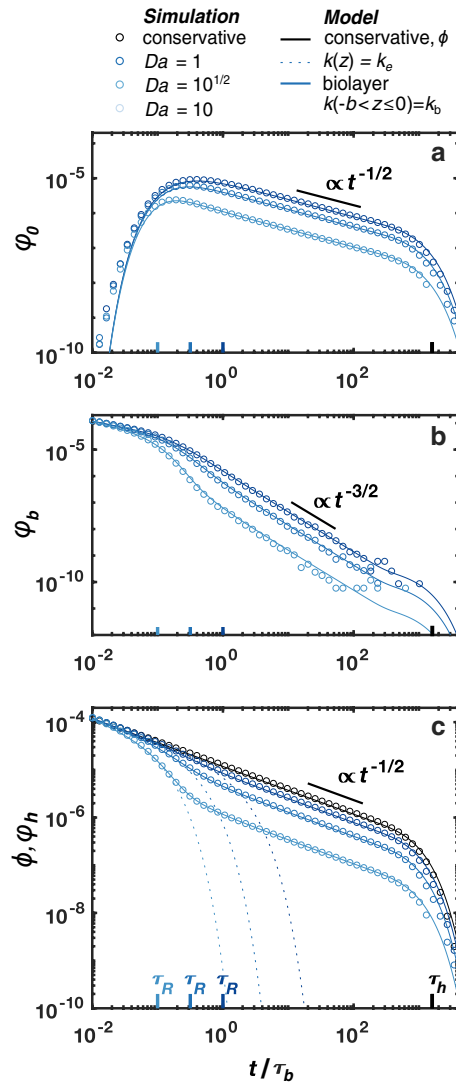


Figure 2. Modeled and simulated memory functions of varying biolayer Da . (a) Memory functions for the inert sublayer show all mass in $-h \leq z < b$. (b) Memory functions for the benthic biolayer show all mass in $-b \leq z < 0$. (c) Full memory functions for conservative (black) and reactive (colored) solutes. Model and simulations transition to $t^{-1/2}$ tailing for $t \gg \tau_b(1 + Da)^{-1}$. For all experiments, $b = 0.05$ m, $D_h = 1.042 \times 10^{-6}$ m²s⁻¹, $h = -2$ m, and k_b is varied. Note that $\tau_e \approx \tau_h$ for all experiments.

$$K_r = \frac{\bar{v}}{2D^*} \left(\sqrt{1 + \frac{4k_a D^*}{\bar{v}^2}} - 1 \right). \quad (7)$$

Equation 7 simplifies to $K_r = k_a \bar{v}^{-1}$ in the limit $D^* \rightarrow 0$, meaning that M_r decays as $\exp(-\tau_a k_a)$ in this limit, where $\tau_a = x \bar{v}^{-1}$ is the advective travel time. Note that K_r is not a reaction rate. It facilitates the estimation of reach-scale mass removal integrated over all times. This is important to note because the time scales for reaction can be very large due to mass transfer limitation in the HZ, which has a dramatic impact on contaminant removal and secondary release as discussed below. Evaluation of K_r is one of several methods that are often inter-compared to determine reach-scale reactivity (e.g., Finkler et al., 2021). For ease of interpretation, we present reach-scale reactivity as uptake velocities, which are commonly used for comparison across rivers. The inverse of K_r denotes the nutrient spiraling length $S_w = K_r^{-1}$ [L], which describes the characteristic distance solute travels downstream before reacting. The uptake velocity $v_f = K_r \bar{v} d$ [L T⁻¹] measures demand for reactants relative to in-stream concentration (Tank et al., 2008).

3. Results and Discussion

3.1. Interplay Between Biolayer Structure and Solute Fate in the HZ

Memory functions, which quantify the mass in the HZ resulting from an instantaneous solute pulse at the SWI, are shown in Figure 2 for (a) the sublayer, (b) the biolayer, and (c) the entire HZ, obtained from the direct numerical simulations and the analytical MIM-B. The sublayer memory function ϕ_0 increases from 0 to a maximum on the time scale τ_b , which is the time for solute transmission across the biolayer. It then decreases as $t^{-1/2}$, as for a conservative solute, due to diffusion back to the biolayer. Last, it tempers exponentially on the time scale τ_e as the sublayer depletes by diffusion.

The memory function ϕ_b for the biolayer decays as $t^{-1/2}$ for times smaller than the reaction time, $t < \tau_R$, due to diffusion across the SWI. For $\tau_R < t < \tau_b$ mass is depleted from the biolayer by reaction, which manifests as an exponential decrease of ϕ_b (Figure 2b). For times $t \gg \tau_b$, the biolayer can be considered well mixed, and ϕ_b transitions to a $t^{-3/2}$ decay because mass in the biolayer changes in a quasi-static fashion due to mass flux from the sublayer (see SI-II D in the Supporting Information S1),

$$\phi_b(t) = -\frac{\tau_b}{1 + Da} \frac{d\phi_0}{dt} \propto t^{-3/2}. \quad (8)$$

The memory function ϕ_h integrates the diffusion-reaction process in the biolayer and retention in the sublayer (Figure 2c). For times $t \ll \tau_R$, mass removal in the streambed is primarily caused by diffusion upward across the SWI, and we observe the characteristic $t^{-1/2}$ decay of a conservative solute. As discussed above, solute is depleted by reaction in the biolayer for $\tau_R < t < \tau_b$, giving rise to an exponential decay of ϕ_h . For $t < \tau_b$ all remaining mass resides at shallow depth in the benthic biolayer, and the system behaves as a scenario of constant streambed reactivity. For $t > \tau_b$, however, solute diffuses into the inert sublayer. Eventually, most mass remaining in the streambed is sequestered below the biolayer. The upward diffusion of mass from the inert sublayer into the biolayer results in a second regime of $\phi_h(t) \sim t^{-1/2}$ (Figure 2c) because diffusion from the sublayer through the biolayer and to the stream is the dominant depletion process. Exponential tempering of $\phi_h(t)$ then occurs on the time scale τ_e (Figure 2c). For comparison, we show memory functions for the corresponding surrogate model SI parameterized with k_e (Figure 2c dotted line). It decays as $t^{-1/2}$ for times smaller than the reaction time $\tau_e = k_e^{-1}$ and exponentially fast for $t > \tau_e$ as solute

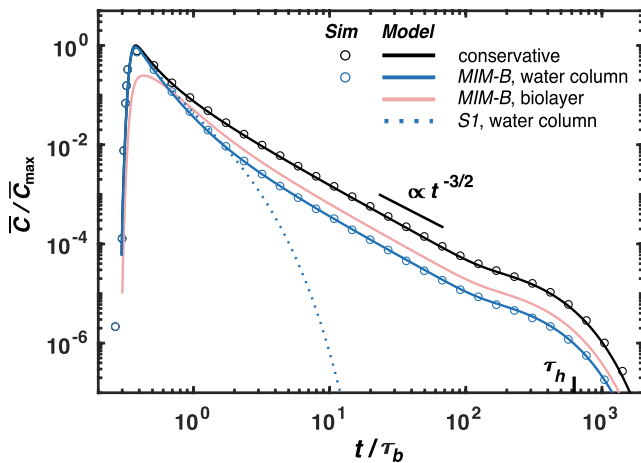


Figure 3. Simulated and MIM-B predicted BTCs for a pulse tracer injection with $x = 100$ m and $b = 0.08$ m, corresponding to $Da = 1.2$. See Section SI-VI in the Supporting Information S1 for other parameter values. \bar{C}_{\max} equals maximum concentration of the analytical solution for the conservative BTC.

degrades throughout the HZ. Thus, *SI* predicts much faster depletion of reactant than the MIM-B because it does not account for long survival in the sublayer.

In summary, the interaction of reaction and diffusion processes in the HZ is governed by three distinct timescales: the characteristic reaction time $\tau_R = k_b^{-1}$, which sets the time for solute depletion from the biolayer by reaction; the diffusion time τ_b , which sets the time for solute transmission through the biolayer to the inert sublayer; and τ_c , which sets the time for diffusive depletion of solute from the sublayer. The match between simulated and modeled memory functions shows that the MIM-B exactly captures the long survival times in the HZ and the spatial segregation of reactants between the biolayer and the non-reactive sublayer.

3.2. Reach-Scale Observations and Model Predictions

3.2.1. Breakthrough Curves

Figure 3 shows BTCs from numerical simulations and MIM-B model predictions, as well as the MIM-B prediction for the biolayer concentration at a control plane 100 m downstream from the injection point. These results are compared to the prediction of surrogate model *SI* for a fully reactive HZ. The

conservative BTC decays as a power law with $t^{-3/2}$ and is cut off at the characteristic diffusion time across the HZ. This behavior is characteristic of diffusive mass transfer and secondary release from the HZ. The BTC for the reactive solute shows the same tailing features as the conservative BTC, albeit at lower concentrations due to degradation in the biolayer. The strong tailing of contaminant concentration is caused by transmission of unreacted solute to the sublayer and release back into the stream through the biolayer. These behaviors are correctly quantified by the MIM-B, which predicts a similar evolution of contaminant concentration in the biolayer (Figure 3 red line), showing that both the stream and the biolayer are sourced by upward diffusion of solute sequestered in the sublayer. Results mirror results from memory function simulations (Figure 2), demonstrating that biolayer structure has a similar influence on degradation timescales at both the local scale and the whole-stream scale. In contrast, *SI* predicts exponential decay of the BTC on the reaction timescale and thus severely under-predicts late time contaminant levels.

The exact match between simulated BTCs and MIM-B predictions demonstrates that the MIM-B fully captures the impact of long survival times in the HZ, as well as the spatial segregation of reactants in the HZ, on reach scale transport and degradation. Notably, the model predicts a power law decay of survival times for all Da . This indicates the potential of MIM-B to provide correct estimates of trace contaminants in benthic sediments and the stream over a range of different physical and chemical conditions in the HZ. Trace organic contaminants (TOCs) are now detected in most rivers (Bernhardt et al., 2017) and impair stream ecosystems at low levels, for example, endocrine disrupting compounds that alter fish physiology at nanomolar concentrations (Khanal et al., 2006). Degradation rates of TOCs decrease rapidly with depth in the HZ and span a range of half lives (Kunkel & Radke, 2008; Schaper et al., 2019). These characteristics allow TOCs to persist in sediments long after they enter the river network and act as a secondary source (Ciparis et al., 2012; Cozzarelli et al., 2017), indicating that their degradation timescales must be estimated by explicitly accounting for the vertically varying reaction rates in the HZ (see SI-VII in the Supporting Information S1).

3.2.2. Reach-Scale Reactivity

The uptake velocity v_f is a common measure of whole-stream reactivity that is based on integration of the simulated BTC (Tank et al., 2008). Calculated v_f agrees well with the analytical prediction from the MIM-B model (Equation 7, Figure 4). The plot also shows that v_f approaches an asymptotic value for values b larger than the characteristic survival depth $s = (D_h/k_b)^{1/2}$, which denotes the diffusion length during the reaction times τ_R . This implies that the spatial extent of the biolayer has little bearing on whole-stream reactivity when $b \gg s$, and nearly all solute reacts before propagating below the biolayer. In contrast, a substantial amount of mass propagates through the biolayer unreacted when $b < s$, resulting in a lower effective reactivity of the HZ (see SI-VII in the Supporting Information S1) and a lower reach-scale reactivity.

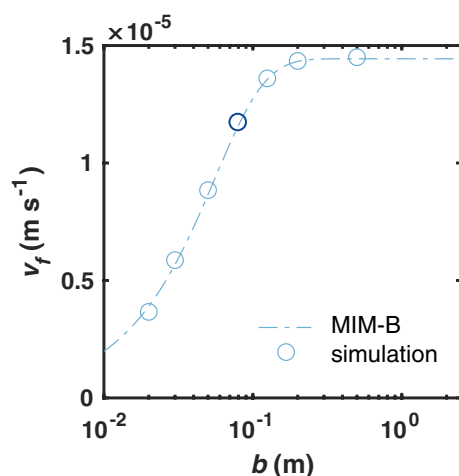


Figure 4. Reach-scale reactivity reported as uptake velocity, for streambeds containing biolayers with varying b . The reaction rate is $k_b = 2.0 \times 10^{-4} \text{ s}^{-1}$ and corresponds to a characteristic survival depth of $s = 0.07 \text{ m}$. See Section SI-VI in the Supporting Information S1 for all parameter values. Dark blue circle is result from the simulation shown in Figure 3.

The MIM-B gives exact estimates of reach-scale reactivity under the assumed conditions of diffusion dominated transport and stratified reactivity in the HZ. It should be emphasized that these estimates are only valid when made at asymptotic times. Transient storage in the HZ delays transport through the reach, causing mass to arrive significantly later than the advective timescale $\tau_a = x \bar{v}^{-1}$, upon which metrics such as v_f are typically based. This delay can cause time-resolved methods for estimating reach-scale reactivity to deviate systematically from the reactivity calculated from integrated mass transformation. For example, results from pulse tracer injection experiments are commonly used to calculate a different effective reaction rate for each data point of the BTC, wherein the reaction time is set to the breakthrough time (Covino et al., 2010). Effective reaction rates calculated from this method depend nonlinearly on reactant concentration even when reactions within the reach are linear, which may lead to the conclusion that reaction kinetics are nonlinear (Li et al., 2021). Integrated methods, such as integration of the BTC or constant rate injection experiments, account for the transport and reaction delays associated with non-local transport to the HZ and mass sequestration below the biolayer. Nevertheless, using these methods may require very long observation times in order to account for the power law decay of reactive mass released from the sublayer, and they provide no information about when concentrations may exceed critical thresholds. Finally, it is important to note that no integrated method gives information on local reaction kinetics or the

time evolution of downstream contaminant concentration. The derived upscaled MIM-B shows that reaction kinetics are in fact non-local as expressed by the right side of Equation 2 and characterized by a power-law decay of contaminant survival times.

4. Conclusion

Two fundamental challenges for providing mechanistic predictions of river corridor reactivity are to explicitly link local heterogeneity of the controlling physical processes to upscaled observations within a consistent modeling framework, and to identify the relative importance of different structural features of the river corridor (Ward & Packman, 2019). We address these challenges by analyzing and upscaling reactive transport in a stream-streambed system characterized by a benthic biolayer. Isolating the dominant small scale features, we derive a novel upscaled model (MIM-B) that captures the dominant physical and chemical processes in the benthic biolayer, the HZ, and reach scale. The model predictions closely agree with direct numerical simulations of a pulse injection experiment in the river. Further, the linearity of the model allows it to flexibly accommodate alternative boundary conditions, such as those associated with non-point source contaminant inputs.

We find that biolayer structure strongly controls solute degradation in the HZ and at the reach scale. Accumulation in the sublayer leads to long survival times for reactive solute, characterized by a power-law decay of concentration and by the spatial segregation of mass in the HZ. This finding is in stark contrast to model predictions based on the classical assumption of a fully reactive HZ, for which exponentially fast decay of concentrations strongly under-predicts contaminant levels in the tail. The novel MIM-B captures all aspects of contaminant degradation on the HZ and reach scales. Specifically, it predicts tail concentrations and reach scale reactivity. Reach scale reactivity quantifies the reaction potential of the stream-streambed system; however, this potential can in principle only be observed at very long experimental times because the sublayer acts as a long-term secondary source.

Although we assume solutes diffuse vertically through the HZ to align our model with empirical scaling laws, we expect similar qualitative behavior in any streambed with vertically varying reaction rates and a multiscale residence time distribution (e.g., Elliott & Brooks, 1997). Furthermore, we conjecture that the sequestration of reactants in non-reactive or less reactive sublayers will dominate the system reactivity also for more complex biogeochemical reaction networks.

The characteristics of reactant fate identified within our model framework are critical for assessing contamination levels in streams and in shallow sediments, which are dramatically underestimated at late times by classical models that assume uniform reaction rates in the hyporheic zone.

Data Availability Statement

Scripts used for direct numerical simulation and figure generation are publicly available (Roche, 2022).

Acknowledgments

KRR was supported by a junior scholar fellowship to Spain from the Fulbright Program. MD acknowledges the support of the Spanish Ministry of Science and Innovation (project HydroPore PID2019-106887GB-C31). High-performance computing support of the R2 (<https://doi.org/10.18122/B2S41H>) and Borah (<https://doi.org/10.18122/oit/3/boisestate>) computer clusters was provided by Boise State University's Research Computing Department. We thank Associate Editor Rose Cory and two anonymous reviewers whose comments improved the quality of the manuscript.

References

- Azizian, M., Grant, S. B., Kessler, A. J., Cook, P. L. M., Rippey, M. A., & Stewardson, M. J. (2015). Bedforms as biocatalytic filters: A pumping and streamline segregation model for nitrate removal in permeable sediments. *Environmental Science & Technology*, 49(18), 10993–11002. <https://doi.org/10.1021/acs.est.5b01941>
- Battin, T. J., Kaplan, L. A., Findlay, S., Hopkinson, C. S., Marti, E., Packman, A. I., et al. (2008). Biophysical controls on organic carbon fluxes in fluvial networks. *Nature Geoscience*, 1(2), 95–100. <https://doi.org/10.1038/ngeo101>
- Bernhardt, E. S., Rosi, E. J., & Gessner, M. O. (2017). Synthetic chemicals as agents of global change. *Frontiers in Ecology and the Environment*, 15(2), 84–90. <https://doi.org/10.1002/fee.1450>
- Ciparis, S., Iwanowicz, L. R., & Voshell, J. R. (2012). Effects of watershed densities of animal feeding operations on nutrient concentrations and estrogenic activity in agricultural streams. *Science of the Total Environment*, 414, 268–276. <https://doi.org/10.1016/j.scitotenv.2011.10.017>
- Covino, T. P., McGlynn, B. L., & McNamara, R. A. (2010). Tracer additions for spiraling curve characterization (TASCC): Quantifying stream nutrient uptake kinetics from ambient to saturation. *Limnology and Oceanography: Methods*, 8(9), 484–498. <https://doi.org/10.4319/lom.2010.8.484>
- Cozzarelli, I. M., Skalak, K. J., Kent, D. B., Engle, M. A., Benthem, A., Mumford, A. C., et al. (2017). Environmental signatures and effects of an oil and gas wastewater spill in the Williston Basin, North Dakota. *Science of the Total Environment*, 579, 1781–1793. <https://doi.org/10.1016/j.scitotenv.2016.11.157>
- Dentz, M., Guze, P., & Carrera, J. (2011). Effective non-local reaction kinetics for transport in physically and chemically heterogeneous media. *Journal of Contaminant Hydrology*, 120–121, 222–236. <https://doi.org/10.1016/j.jconhyd.2010.06.002>
- Dodds, W. K., López, A. J., Bowden, W. B., Gregory, S., Grimm, N. B., Hamilton, S. K., et al. (2002). N uptake as a function of concentration in streams. *Journal of the North American Benthological Society*, 21(2), 206–220. <https://doi.org/10.2307/1468410>
- Elliott, A. H., & Brooks, N. H. (1997). Transfer of nonsorbing solutes to a streambed with bed forms: Theory. *Water Resources Research*, 33(1), 123–136. <https://doi.org/10.1029/96WR02784>
- Finkler, N. R., Glücker, B., Boëchat, I. G., Tromboni, F., Thomas, S. A., Mendes, L. A., et al. (2021). Comparing spiraling- and transport-based approaches to estimate in-stream nutrient uptake length from pulse additions. *Ecohydrology*, e2331.
- Fischer, H. B., List, J. E., Koh, C. R., Imberger, J., & Brooks, N. H. (1979). *Mixing in inland and coastal waters*. Academic press.
- Garayburu-Caruso, V. A., Stegen, J. C., Song, H.-S., Renteria, L., Wells, J., Garcia, W., et al. (2020). Carbon limitation leads to thermodynamic regulation of aerobic metabolism. *Environmental Science & Technology Letters*, 7, 517–524. <https://doi.org/10.1021/acs.estlett.0c00258>
- Grant, S. B., Stewardson, M. J., & Marusic, I. (2012). Effective diffusivity and mass flux across the sediment-water interface in streams: Effective diffusion coefficient for hyporheic exchange. *Water Resources Research*, 48(5). <https://doi.org/10.1029/2011WR011148>
- Haggerty, R., Marti, E., Argerich, A., von Schiller, D., & Grimm, N. B. (2009). Resazurin as a “smart” tracer for quantifying metabolically active transient storage in stream ecosystems. *Journal of Geophysical Research*, 114(G3), G03014. <https://doi.org/10.1029/2008JG000942>
- Haggerty, R., Wondzell, S. M., & Johnson, M. A. (2002). Power-law residence time distribution in the hyporheic zone of a 2nd-order mountain stream. *Geophysical Research Letters*, 29(13), 1640. <https://doi.org/10.1029/2002gl014743>
- Harvey, J. W., Böhlke, J. K., Voytek, M. A., Scott, D., & Tobias, C. R. (2013). Hyporheic zone denitrification: Controls on effective reaction depth and contribution to whole-stream mass balance: Scaling hyporheic flow controls on stream denitrification. *Water Resources Research*, 49(10), 6298–6316. <https://doi.org/10.1002/wrcr.20492>
- Inwood, S. E., Tank, J. L., & Bernot, M. J. (2007). Factors controlling sediment denitrification in midwestern streams of varying land use. *Microbial Ecology*, 53(2), 247–258. <https://doi.org/10.1007/s00248-006-9104-2>
- Jones, J. B., & Mulholland, P. J. (1999). *Streams and ground waters*. Academic Press.
- Khanal, S. K., Xie, B., Thompson, M. L., Sung, S., Ong, S.-K., & van Leeuwen, J. H. (2006). Fate, transport, and biodegradation of natural estrogens in the environment and engineered systems. *Environmental Science & Technology*, 40(21), 6537–6546. <https://doi.org/10.1021/es0607739>
- Knapp, J. L. A., González-Pinzón, R., Drummond, J. D., Larsen, L. G., Cirpka, O. A., & Harvey, J. W. (2017). Tracer-based characterization of hyporheic exchange and benthic biolayers in streams: Hyporheic exchange and benthic biolayers. *Water Resources Research*, 53(2), 1575–1594. <https://doi.org/10.1002/2016WR019393>
- Kunkel, U., & Radke, M. (2008). Biodegradation of acidic pharmaceuticals in bed sediments: Insight from a laboratory experiment. *Environmental Science & Technology*, 42(19), 7273–7279. <https://doi.org/10.1021/es801562j>
- Li, A., Aubeneau, A. F., Bolster, D., Tank, J. L., & Packman, A. I. (2017). Covariation in patterns of turbulence-driven hyporheic flow and denitrification enhances reach-scale nitrogen removal: Hyporheic flow-denitrification upscaling. *Water Resources Research*, 53(8), 6927–6944. <https://doi.org/10.1002/2016WR019949>
- Li, A., Bernal, S., Kohler, B., Thomas, S. A., Marti, E., & Packman, A. I. (2021). Residence time in hyporheic bioactive layers explains nitrate uptake in streams. *Water Resources Research*, 57(2), e2020WR027646. <https://doi.org/10.1029/2020WR027646>
- Marzadri, A., Dee, M. M., Tonina, D., Bellin, A., & Tank, J. L. (2017). Role of surface and subsurface processes in scaling N₂O emissions along riverine networks. *Proceedings of the National Academy of Sciences*, 114(17), 4330–4335. <https://doi.org/10.1073/pnas.1617454114>
- Moran, P. W., Nowell, L. H., Kemble, N. E., Mahler, B. J., Waite, I. R., & Van Metre, P. C. (2017). Influence of sediment chemistry and sediment toxicity on macroinvertebrate communities across 99 wadable streams of the Midwestern USA. *Science of the Total Environment*, 599–600, 1469–1478. <https://doi.org/10.1016/j.scitotenv.2017.05.035>
- Reeder, W. J., Quick, A. M., Farrell, T. B., Benner, S. G., Feris, K. P., Marzadri, A., & Tonina, D. (2018). Hyporheic source and sink of nitrous oxide. *Water Resources Research*, 54(7), 5001–5016. <https://doi.org/10.1029/2018WR022564>

- Roche, K. (2022). Supplementary files for “Benthic biolayer structure controls whole-stream reactive transport”. <https://doi.org/10.6084/m9.figshare.19011686.v1>
- Roche, K. R., Shogren, A. J., Aubeneau, A., Tank, J. L., & Bolster, D. (2019). Modeling benthic versus hyporheic nutrient uptake in unshaded streams with varying substrates. *Journal of Geophysical Research: Biogeosciences*, 124(2), 367–383. <https://doi.org/10.1029/2018JG004684>
- Runkel, R. L. (2007). Toward a transport-based analysis of nutrient spiraling and uptake in streams. *Limnology and Oceanography: Methods*, 5(1), 50–62. <https://doi.org/10.4319/lom.2007.5.50>
- Russian, A., Dentz, M., & Gouze, P. (2016). Time domain random walks for hydrodynamic transport in heterogeneous media. *Water Resources Research*, 52(5), 3309–3323. <https://doi.org/10.1002/2015wr018511>
- Schaper, J. L., Posselt, M., Bouchez, C., Jaeger, A., Nuetzmann, G., Putschew, A., et al. (2019). Fate of trace organic compounds in the hyporheic zone: Influence of retardation, the benthic biolayer, and organic carbon. *Environmental Science & Technology*, 53(8), 4224–4234. <https://doi.org/10.1021/acs.est.8b06231>
- Tank, J. L., Rosi-Marshall, E. J., Baker, M. A., & Hall, R. O. (2008). Are rivers just big streams? A pulse method to quantify nitrogen demand in a large river. *Ecology*, 89(10), 2935–2945. <https://doi.org/10.1890/07-1315.1>
- Ward, A. S., & Packman, A. I. (2019). Advancing our predictive understanding of river corridor exchange. *WIREs Water*, 6(1), e1327. <https://doi.org/10.1002/wat2.1327>